XIV International Conference on Computational Plasticity. Fundamentals and Applications
COMPLAS XIV
E. Oñate, D.R.J. Owen, D. Peric & M. Chiumenti (Eds)

PHENOMENOLOGICAL MODELING OF STRAIN HARDENING, PHASE TRANSFORMATION AND DAMAGE EFFECTS OF TRIP-STEELS

ANDREAS SEUPEL AND MEINHARD KUNA

TU Bergakademie Freiberg
Institute of Mechanics and Fluid Dynamics
Lampadiusstraße 4, 09599 Freiberg, Germany
e-mail: Andreas.Seupel@imfd.tu-freiberg.de, web page: http://www.tu-freiberg.de/

Key words: TRIP-steel, Asymmetric Strain Hardening, Non-local Damage Model

Abstract. In this study, the constitutive modeling of loading state dependent strain hardening and martensite evolution of high alloyed TRIP-steels are addressed, which are experimentally observed comparing uni-axial tension and compression test results. Furthermore, a damage mechanics extension of the model is proposed, which is based on the continuum damage mechanics framework. An implicit gradient based enrichment method is applied to realize a non-local damage formulation. For the implementation into the commercial FEM-software ABAQUS, the analogy between the additional Helmholtz-type equation of implicit gradient enrichment and the already built-in heat conduction equation is used. Finally, the developed model is fitted to experimental data and cell model calculations. A convergence study using the non-local extension is discussed.

1 INTRODUCTION

Metastable austenitic steels exhibit outstanding strain hardening and ductility properties due to a martensitic phase transformation during thermo-mechanical loading. The typical strain hardening behavior and the additional plastic deformations caused by phase transition are often summarized as TRIP-effect (TRansformation Induced Plasticity).

In this paper, we focus on the mechanical behavior of a special TRIP-steel considering its stress state dependent material response. Starting point is the experimental observation of asymmetric strain hardening and martensite evolution under uni-axial tension and compression loading. We propose a model, which comprises both features. Similar effects are extensively discussed in literature (see e. g. [1, 2]).

Furthermore, the description of the material's failure is addressed. Existing local approaches to fracture for TRIP-steels (see [3, 4]) suffer from their well known mesh dependency in finite element computations. Therefore, a continuum damage mechanics model with non-local regularization is also proposed in this paper to include failure into the developed constitutive model of TRIP-steel.

The modeling approaches are successively applied: (i) The plasticity model is fitted to tension and compression experiments conducted for a high alloyed TRIP-steel. (ii) The proposed damage extension of the model is calibrated and tested with help of cell model simulations of TRIP-steel containing micro-voids. (iii) The mentioned regularization method is investigated by means of a convergence study.

Notation hints: Tensors are subsequently introduced. Symbolic notation is used, where scalars are denoted italic A, first order tensors as $\vec{A}$, second order tensors as bold symbols $\boldsymbol{A}$ and fourth order tensor are highlighted calligraphically $\mathcal{A}$. Single and double contraction of tensors are denoted by '$\cdot$' and ':', respectively.

2 PROPOSED MODEL

2.1 Stress-strain relation

Starting with an additive split of the rate of deformation tensor $\boldsymbol{D}$ into an elastic, plastic and a transformation induced part

$$\boldsymbol{D} = \boldsymbol{D}_{\mathrm{el}} + \boldsymbol{D}_{\mathrm{pl}} + \boldsymbol{D}_{\mathrm{tr}}, \tag{1}$$

we assume the following hypo-elastic relation between the Kirchhoff-stress tensor $\hat{\boldsymbol{\tau}}$ and the elastic part of the rate of deformation tensor:

$$(\hat{\boldsymbol{\tau}})^{\circ} = \mathcal{C} : \boldsymbol{D}_{\mathrm{el}}. \tag{2}$$

In the previous and following equations, a hat ($\hat{\cdot}$) highlights an effective (undamaged) value. The objective time derivative of the Kirchhoff-stress tensor is denoted by $(\cdot)^{\circ}$, where the Jaumann-rate is used in what follows. The fourth-order tensor of isotropic, linear elastic stiffness is denoted by $\mathcal{C}$. The relation between the Kirchhoff-stress tensor $\hat{\boldsymbol{\tau}}$ and the Cauchy-(true)-stress tensor $\hat{\boldsymbol{\sigma}}$ reads

$$\hat{\boldsymbol{\tau}} = \det(\boldsymbol{F})\, \hat{\boldsymbol{\sigma}}, \tag{3}$$

with the deformation gradient $\boldsymbol{F}$.

2.2 TRIP-effect: martensite evolution, kinematics and strain hardening

The evolution of strain induced martensite (volume fraction z) is based on the Olson-Cohen-model (see [5])

$$\dot{z} = (1 - z)\, \beta n f_{\mathrm{sb}}^{n-1} \dot{f}_{\mathrm{sb}}, \tag{4}$$

where $\dot{f}_{\mathrm{sb}}$ denotes the volume fraction of shear bands, which act as nucleation sites for martensite. The probability of forming a martensite nucleus at crossing points of shear bands is included in the parameter β, whereas n is a geometrical constant. The shear band volume fraction is assumed to obey the evolution law

$$\dot{f}_{\mathrm{sb}} = \alpha\, (1 - f_{\mathrm{sb}})\, \dot{\varepsilon}_{\mathrm{eq}}. \tag{5}$$

The entire martensite evolution is driven by the plastic deformation (equivalent plastic strain $\varepsilon_{\mathrm{eq}}$). Former studies propose a dependency of the shear band rate α and the probability parameter β on temperature, strain rate and stress state (see e. g. [6]). We focus on the stress state dependency only. The stress state of uni-axial tension and compression loadings can be distinguished by the stress triaxiality h

$$h = \frac{I_1}{3\sqrt{3J_2}} \tag{6}$$

and the Lode-parameter

$$\cos(3\phi) = \frac{3\sqrt{3}}{2}\frac{J_3}{J_2^{\frac{3}{2}}}, \qquad -1 \leq \cos(3\phi) \leq 1. \tag{7}$$

The necessary invariants of the stress tensor $\hat{\boldsymbol{\tau}}$ to calculate the former values are the first invariant of the stress tensor I_1 as well as the second and third invariant of the stress deviator $\hat{\boldsymbol{S}}$, J_2 and J_3, respectively. At this stage of investigation, a primary influence of the stress triaxiality h on martensite formation is considered. The ansatz for the triaxiality dependent parameter α reads:

$$\alpha(\hat{\boldsymbol{\tau}}) = \alpha_0 + \alpha_1 \left(\frac{2}{\pi} \arctan(h\,\alpha_2) + 1 \right). \tag{8}$$

To ensure $\alpha \geq 0$, the restrictions $\alpha_0 \geq 0$ and $\alpha_1 \geq -\frac{\alpha_0}{2}$ apply. An analogous term is used to define $\beta(\hat{\boldsymbol{\tau}})$ with upcoming parameters β_0, β_1 and β_2. Therewith, a triaxiality influence occurs, but the values of α and β are limited for $h \to (-\infty, +\infty)$. An additional term containing the Lode-parameter $\cos(3\phi)$ can be added to delineate further loading states (see [1]).

The martensite evolution leads to additional inelastic deformations on the macroscopic scale (TRIP-strains). Besides deviatoric contributions, also a volume change can be detected. The rate of deformation tensor related to phase transformation is introduced as

$$\boldsymbol{D}_{\mathrm{tr}} = M\boldsymbol{N}\dot{z} + \frac{1}{3}\triangle_{\mathrm{v}}\boldsymbol{\delta}\dot{z}. \tag{9}$$

This postulates, that the transformation strains are proportional to the martensite volume fraction and that the deviatoric part has the direction of the yield normal $\boldsymbol{N}$ associated with the conventional plastic flow. The unity tensor related to the volumetric part is denoted as $\boldsymbol{\delta}$. The amount of shearing and volume change due to martensite evolution is controlled by the parameters M and $\triangle_{\mathrm{v}}$.

The martensite formed during deformation apparently affects the strain hardening behavior (i. e. typical sigmoidal hardening curves). The physical hardening mechanisms resulting from dislocation-martensite interactions are illustrated elsewhere for the considered steel (see [7]). A phenomenological contribution to the isotropic hardening of the material is applied

$$\tau_{\mathrm{m}}(z) = Z_1\left(\exp(Z_2 z) - 1\right), \tag{10}$$

containing two parameters (Z_1, Z_2).

2.3 Elasto-plasticity with asymmetric strain hardening

From multi-axial testing of the considered TRIP-steel, the von Mises yield criterion was found to be appropriate to describe the initial yield stress (see [8]). Therefore, the modeling is based on the yield function

$$y = \tau_{\mathrm{eq}} - R\left(r\right) - \tau_{\mathrm{m}}\left(z\right) - \tau_0 \leq 0, \tag{11}$$

in the framework of rate independent plasticity. Only an isotropic hardening is considered with contributions due to martensite evolution $\tau_{\mathrm{m}}\left(z\right)$ and dislocation based mechanisms $R\left(r\right)$. An asymmetry of the strain hardening between uni-axial tension and compression can be caused by the martensite contribution. Due to the proposed martensite evolution approach, more martensite is formed during tensile loading, i. e. the flow stress should be higher than under compressive loading at comparable strains. But a higher flow stress is experimentally observed during uni-axial compression (see Fig. 1). Therefore, the hardening variable r is defined as follows: Firstly, an associated flow rule for the plastic rate of deformation tensor is utilized

$$\boldsymbol{D}_{\mathrm{pl}} = \dot{\Lambda}\frac{\partial y}{\partial \hat{\boldsymbol{\tau}}} = \dot{\Lambda}\boldsymbol{N} \tag{12}$$

$$\boldsymbol{N} = \frac{3}{2\tau_{\mathrm{eq}}}\hat{\boldsymbol{S}}. \tag{13}$$

One finds an expression for the equivalent plastic strain rate and the relation to the Lagrangian multiplier $\dot{\Lambda}$ in the well known manner:

$$\dot{\varepsilon}_{\mathrm{eq}} = \sqrt{\frac{2}{3}\boldsymbol{D}_{\mathrm{pl}} : \boldsymbol{D}_{\mathrm{pl}}} = \dot{\Lambda}. \tag{14}$$

The hardening variable is now introduced as

$$\dot{r} = \left(1 - G\right)\dot{\varepsilon}_{\mathrm{eq}} \geq 0, \tag{15}$$

where G is assumed to be a function of the Lode-parameter $\cos\left(3\phi\right)$:

$$G\left(\cos\left(3\phi\right)\right) = \frac{B}{2}\left(1 + \cos\left(3\phi\right)\right), \qquad \text{with } 0 \leq B, G < 1. \tag{16}$$

Just the additional parameter B appears. The uni-axial compression test can be seen as reference, because G vanishes. The strain hardening during uni-axial tension can be decreased by finding an appropriate value of $B < 1$. The hardening rule is very flexible, because it can be easily extended by dependencies on z or $\varepsilon_{\mathrm{eq}}$. Considering an effect of the Lode-parameter on strain hardening implies an orientation influence, which has to be clarified in future investigations.

The hardening function is assembled by the case differentiation

$$R = \begin{cases} Hr^q & ,r \leq r_{\mathrm{c}} \\ Hr_{\mathrm{c}}^q + R_\infty\left(1 - \exp\left(-\frac{H\,q\,r_{\mathrm{c}}^{q-1}}{R_\infty}\left(r - r_{\mathrm{c}}\right)\right)\right) & ,\text{else.} \end{cases} \tag{17}$$

with the four parameters H, q, r_c and R_∞. This extends the typical power law for hardening to incorporate a saturation after exceeding a critical value r_c.

The elasto-plastic model for TRIP-steel is completed by the Kuhn-Tucker-conditions

$$\dot{\Lambda} \geq 0, \qquad \dot{\Lambda}\, y = 0, \qquad y \leq 0 \tag{18}$$

and the consistency condition

$$\dot{y} = 0. \tag{19}$$

The derived model equations can be numerically solved by standard methods (see [9]). The finite strain formulation, which is based on an updated Lagrange-method combined with an integration of the hypo-elastic equation, is directly provided by the FEM-software (ABAQUS/standard version 6.14).

2.4 Damage model

Starting point of continuum damage mechanics is the effective stress concept leading to

$$\boldsymbol{\sigma} = (1 - D)\, \hat{\boldsymbol{\sigma}}, \tag{20}$$

where $\boldsymbol{\sigma}$ is the macroscopic stress, $\hat{\boldsymbol{\sigma}}$ is the effective stress acting on the undamaged material and D is an isotropic damage variable with $0 \leq D \leq 1$. The damage variable D is typically considered as ratio of damaged area over net area, whereby also the meaning of a porosity is possible.

Damage evolves until reaching a critical value of $D_\mathrm{c} \ll 1$. We interpret this as the beginning of a void coalescence mechanism leading rapidly to the failure of the material. A phenomenological acceleration of damage is taken into account by introducing the modified damage variable D^*:

$$D^* = \begin{cases} D & , D < D_\mathrm{c} \\ D + \kappa \left(D_\mathrm{c} - D\right)^2 & , \text{else.} \end{cases} \tag{21}$$

The acceleration is driven by $\kappa > 0$. In order to realize a smooth transition to the total failure state, a second modification is used after a critical value near failure D_t^* is reached. An exponential type function

$$D^* = D_\mathrm{max}^* \left(1 - \exp\left[-D_2 \left(D - D_3\right)\right]\right), \qquad D^* > D_\mathrm{t}^* \tag{22}$$

is utilized, where the maximum damage value D_max^* and the transition D_t^* can be chosen (choice: $D_\mathrm{max}^* = 0.9999$, $D_\mathrm{t}^* = 0.8$). The other parameters are determined by demanding smooth differentiability at $D^* = D_\mathrm{t}^*$ considering Eqn. (21) and (22):

$$D_1 = \frac{2 D_\mathrm{c} \kappa - 1 + \sqrt{1 + 4\kappa \left(D_\mathrm{t} - D_\mathrm{c}\right)}}{2\kappa} \tag{23}$$

$$D_2 = \frac{1 + 2\kappa \left(D_1 - D_\mathrm{c}\right)}{D_\mathrm{max}^* - D_\mathrm{t}} \tag{24}$$

$$D_3 = D_1 + \frac{1}{D_2} \ln\left[1 - \frac{D_\mathrm{t}}{D_\mathrm{max}^*}\right]. \tag{25}$$

When damage at a material point attains a value $D^* = 1$, a crack is assumed to be initiated. For technical reasons, we declare the criterion $D^* \geq 0.99$ as initiation point.

Typically, failure of steels originates from nucleation, growth and coalescence of micro-voids. Therefore, the Rice and Tracey model of void growth is taken into account (see [10]). The damage (porosity) evolves as

$$\dot{D} = (1 - D)\, \dot{\varepsilon}_\mathrm{d}, \tag{26}$$

where the damage driving strain rate $\dot{\varepsilon}_\mathrm{d}$ is formulated to yield :

$$\dot{\varepsilon}_\mathrm{d} = \begin{cases} D^* K_1 \exp\left(\frac{h}{h_1}\right) \dot{\varepsilon}_\mathrm{dev} & , h < h_\mathrm{t} \text{ and } D < D_\mathrm{c} \\ D^* K_1 e_\mathrm{smooth}\,(h)\, \dot{\varepsilon}_\mathrm{dev} & , h \geq h_\mathrm{t} \text{ and } D < D_\mathrm{c}. \end{cases} \tag{27}$$

Damage is then a function of stress triaxiality h. A scalar measure of deviatoric deformation $\dot{\varepsilon}_\mathrm{dev}$ is introduced, which combines plastic and TRIP-contributions. Its formulation is discussed subsequently. K_1 and h_1 are adjustable parameters. To avoid numerical problems, the exponential term of the Rice and Tracey model is restricted by determining a cut-off triaxiality h_t. The function e_smooth provides a finite value for $h \to \infty$ and contains one additional parameter h_max (see Appendix).

Results of cell model simulations on porous metals show, that a uni-axial straining state occurs after exceeding the critical damage D_c (see e. g. [4]). Therefore, the damage driving strain rate switches to

$$\dot{\varepsilon}_\mathrm{d} = \frac{3}{2}\dot{\varepsilon}_\mathrm{dev}, \qquad D \geq D_\mathrm{c}. \tag{28}$$

We suggest an approximation of the rate of equivalent inelastic strain $\dot{\varepsilon}_\mathrm{dev}$ by the value calculated from the deviatoric part $\boldsymbol{D}_\mathrm{dev}$ of the whole rate of deformation tensor $\boldsymbol{D}$ as:

$$\dot{\varepsilon}_\mathrm{dev} = \begin{cases} \sqrt{\frac{2}{3}\boldsymbol{D}_\mathrm{dev} : \boldsymbol{D}_\mathrm{dev}} & , \dot{\Lambda} > 0 \\ 0 & , \text{ else.} \end{cases} \tag{29}$$

As a result, after computing the effective stress response, damage can be evaluated separately by integrating Eq. (26). Regarding all modifications, Eq. (20) is rewritten as

$$\boldsymbol{\sigma} = (1 - D^*)\, \hat{\boldsymbol{\sigma}}. \tag{30}$$

2.5 Non-local damage model

An implicit gradient regularization method is used to obtain a non-local spatial average of a damage related variable (see e. g. [11]). The deformation and stress dependent damage driving strain rate $\dot{\varepsilon}_\mathrm{d}$ is chosen to be replaced by its non-local counterpart $\dot{\bar{\varepsilon}}_\mathrm{d}$ in the damage evolution law Eq. (26). This ensures, that a fully damaged state $D^* \to D^*_\mathrm{max}$ can be achieved. The non-local variable is determined by solving the additional field equation of Helmholz-type (∇^2 - Laplacian, $\vec{\nabla}$ - Nabla-operator):

$$\bar{\varepsilon}_\mathrm{d} - L^2 \nabla^2 \bar{\varepsilon}_\mathrm{d} = \varepsilon_\mathrm{d}. \tag{31}$$

The regularization involves an additional internal length parameter L. The boundary conditions are chosen as

$$\vec{\nabla}\bar{\varepsilon}_{\mathrm{d}} \cdot \vec{n} = 0, \tag{32}$$

according to [11] ($\vec{n}$ - normal to current boundary).

At this point, some remarks on possible implementation strategies using the FE-code ABAQUS/standard (version 6.14) should be given. The constitutive law is defined via subroutine UMAT. The similarity between the field equation Eq. (31) and the stationary heat equation can be used to avoid implementing a user defined finite element (subroutine UEL). The temperature degree of freedom changes its meaning to the non-local variable $\bar{\varepsilon}_{\mathrm{d}}$. Firstly, a fully thermal-displacement-coupled simulation step with stationary heat transfer has to be defined. Declaring a 'heat generation' r_{pl} in subroutine HETVAL as

$$r_{\mathrm{pl}} = -\bar{\varepsilon}_{\mathrm{d}} + \varepsilon_{\mathrm{d}} \tag{33}$$

changes the heat equation into the desired Helmholtz-equation. The implementation requires also additional material tangent entries, which can be defined in subroutines UMAT and HETVAL. The internal length is provided by defining the 'conductivity' L^2. For the considered 2D-plane strain-problems in section 3.3 we use quadratic shape functions to approximate the displacements and linear shape functions for the non-local variable. A reduced integration scheme is applied (ABAQUS element CPE8RT).

3 RESULTS AND DISCUSSION

Firstly, the results of fitting the TRIP-steel model to experimental data is discussed. No damage is considered at this stage. The chemical composition of the considered TRIP-steel is given in Tab. 1. The uni-axial tensile and compressive tests were conducted at a low temperature (273.15 K) to generate a high amount of martensite during mechanical loading; the experimental techniques can be found in [12]. For measuring the martensite content, the setup described in [13] was used.

Secondly, the *local* damage model is fitted to cell model simulations of TRIP-steel with micro-voids (porosity=1 %). Cell model simulations of porous metals are well known, general information can be found in [14]. The simple case of an axi-symmetric unit cell is used here. During loading, the stress triaxiality h is held constant. Macroscopic stress-strain curves can be extracted. As material model for the metal matrix, the fitted TRIP-steel model without damage is utilized.

Finally, a convergence study using the *non-local* damage model is presented. The considered 2D boundary value problem of a plate with a hole and some kinematic restrictions are sketched in Fig. 2 (symmetry conditions are applied, plane strain state, displacement controlled).

3.1 Fit to uni-axial experiments

As illustrated in Fig. 1, the stress-strain response as well as the martensite evolution of uni-axial compression and tension tests are captured by the proposed model. Espe-

Table 1: Chemical composition of the investigated 16Cr-7Mn-7Ni TRIP-steel (in mass-%)

Fe	C	Cr	Mn	Ni	Al	Si	Mo	Ti	N
bal.	0.02	15.9	7.1	6.9	0.015	1.16	0.025	0.01	0.08

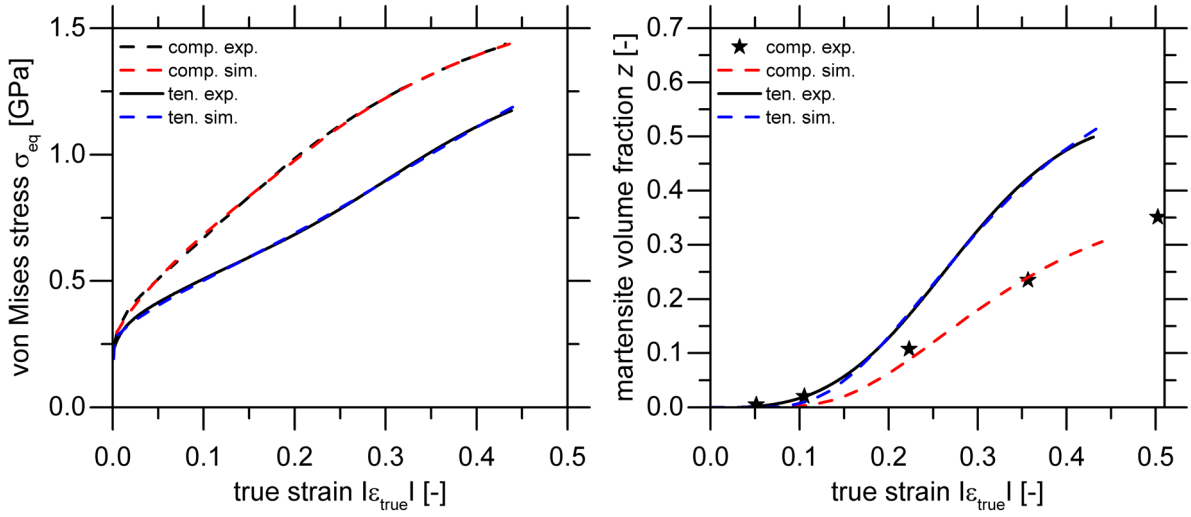

Figure 1: Fitting results of the model (sim.) to uni-axial tension (ten.) and compression (comp.) results (exp.): true stress-strain-curves (lhs) and martensite evolution (rhs)

cially the asymmetric hardening is matched well. During parameter optimization, the martensite evolution parameters can be fitted prior to the hardening parameters.

3.2 Fit to cell model simulation

Prior to the fitting procedure, a convergence study regarding the permissible strain increment during loading was performed. After exceeding D_c, a high sensitivity concerning the strain increment was found. In all upcoming simulations, the possible crossing of D_c is checked during computation at every integration point. The (absolute) biggest component of the strain increment tensor must not exceed 0.001 for $D \geq D_c$.

An initial damage of $D_0 = 0.01$ is applied during the calibration of the damage model to the cell model results. The hardening and martensite evolution parameters are optimized to fit the uni-axial cell model result ($h = 1/3$, see Tab. 2), where damage has a minor influence. Afterwards, the damage parameters K_1, h_1, D_c and κ are calibrated to match the stress-strain behavior of the cell model at higher stress triaxialities (see Tab. 2). According to Fig. 2 (lhs), the qualitative behavior is reasonable. A good agreement is found for $h = 2$, whereas a slight mismatch is visible for $h = 1$ and $h = 3$.

3.3 Numerical example and convergence study

For the convergence study concerning the spatial discretization, the boundary value problem depicted in Fig. 2 (rhs) with the parameter set of Tab. 2 is considered. Five discretization variants are realized, where the ratio of a characteristic element length l_e over

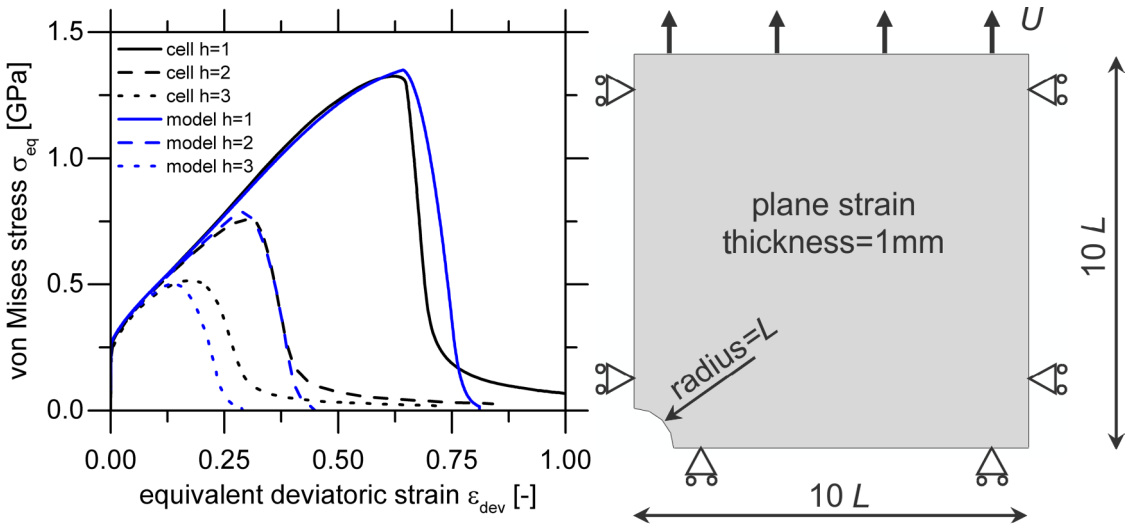

Figure 2: Fitting results of the local damage model to cell model results at three different triaxialities h (equivalent stress - equivalent strain curves of model and cell simulations, lhs) and boundary value problem of the convergence study (plate with hole, rhs)

Table 2: Model and material parameters found from cell model fit (E - Young's modulus, ν - Poisson's ratio, τ_0 - initial yield stress)

E [GPa]	ν [-]	τ_0 [MPa]	H [MPa]	q [-]	r_c [-]	R_∞ [MPa]	Z_1 [MPa]	Z_2 [-]
192	0.24	264.216	2427.952	0.753	0.199	428.93	177.96	1.864
B [-]	M [-]	$\triangle_v$ [-]	α_0 [-]	α_1 [-]	α_2 [-]	β_0 [-]	β_1 [-]	β_2 [-]
0.535	0.12	0.02	0.101	7.006	0.083	0.517	0.272	294.679
n [-]	D_0 [-]	K_1 [-]	h_1 [-]	D_c [-]	κ [-]	h_t [-]	h_{max} [-]	L [mm]
6.037	0.01	1.507	1.21	0.085	30	3	5	0.4

internal length L is systematically varied: $l_e/L = 1/16...1$. Quadrilateral finite elements are utilized; the prescribed edge length is chosen as l_e. The simulation is interrupted, if crack initiation is reached anywhere. Fig. 3 (lhs) shows the global response of the structure for different meshes. A sharp load drop prior to crack growth can be observed. No mesh size dependency exists, where the load drop would clearly occur at different displacements.

The magnified view of the load drop highlights the convergent behavior. The curves for $l_e/L \leq 1/4$ seem to coincide. A quantitative error analysis is performed through defining a relative error

$$\Delta_U = \frac{|U_{ci} - U_{ci,l_e=1/16}|}{U_{ci,l_e=1/16}} \tag{34}$$

of the nominal displacement at crack initiation $U = U_{ci}$ with respect to the finest mesh. Fig. 3 (rhs) reveals that a convergence exists, where the relative error for $l_e/L = 1/4$ is already smaller than 0.1%. This confirms the recommendation to use $l_e/L = 1/4$, which can be found in [11].

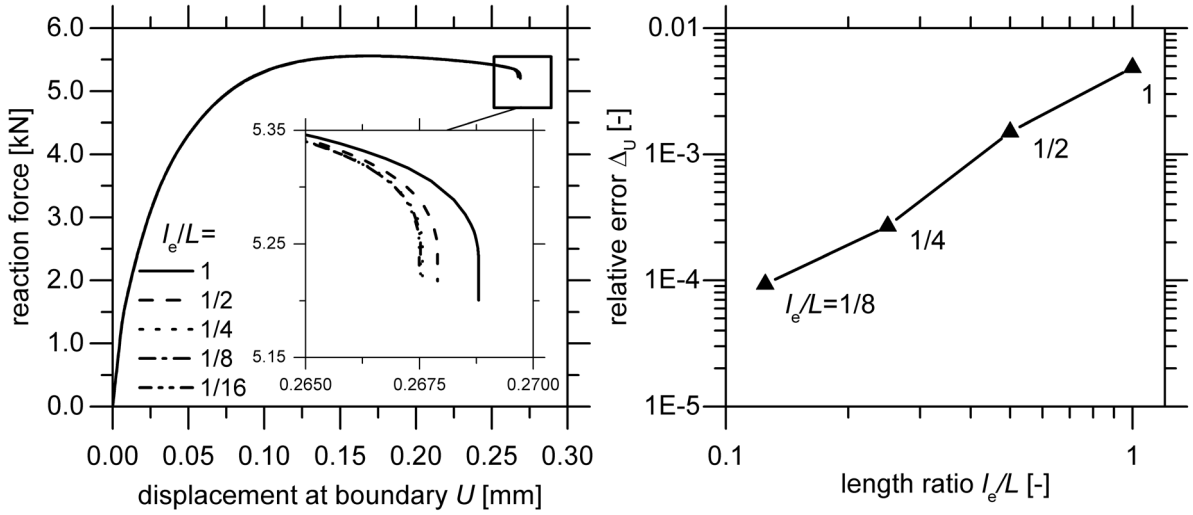

Figure 3: Convergence study results: force-displacement response until crack initiation of different discretization l_e/L (lhs) and relative error analysis of the displacement at crack initiation (rhs)

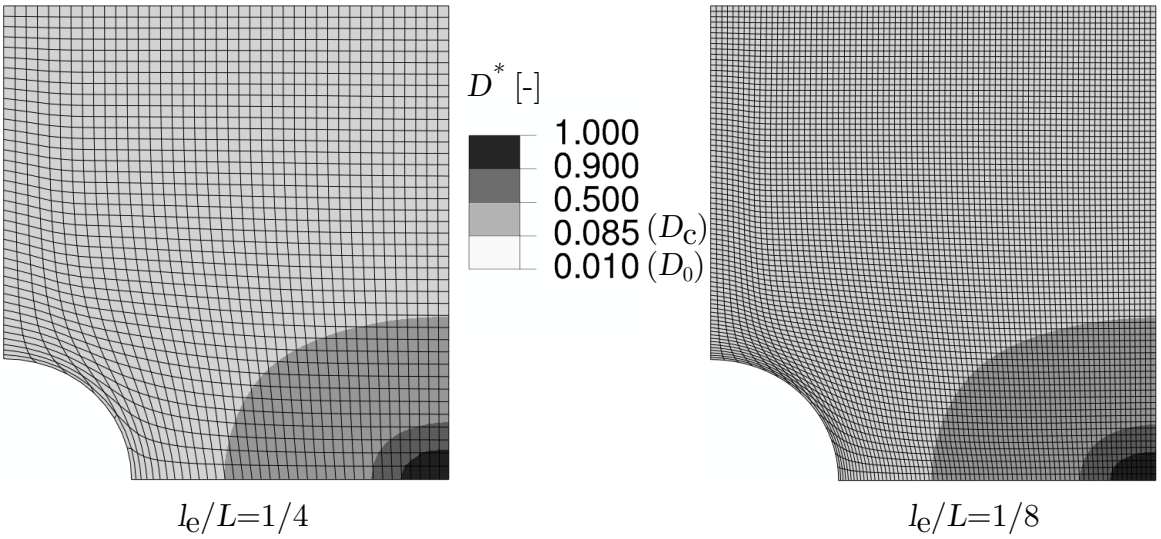

Figure 4: Convergence study results: contour plot of damage D^* at crack initiation point for two meshes $l_\mathrm{e}/L = 1/4$ (lhs) and $l_\mathrm{e}/L = 1/8$ (rhs)

Remark: For the previous convergence study, the change of the damage driving force $\dot{\varepsilon}_\mathrm{d}$ beyond D_c is neglected (see Eq. (28)). We found also mesh independent results for activating this switching, but the convergence behavior was not as 'beautiful' as for the non-switching case.

The local convergence behavior is illustrated by a closer view to the damage distribution at the point of crack initiation (Fig. 4). Two mesh sizes are compared: $l_\mathrm{e}/L = 1/4$ and $l_\mathrm{e}/L = 1/8$. Firstly, the location of damage should be mentioned, which is not directly near the hole, but rather at the right boundary, because higher triaxiality values occur

at this position. Both meshing variants show a qualitatively and quantitatively similar distribution of damage. It can be clearly seen, that the zone of massive damage ($D^* > 0.9$) is spread over some layers of elements, especially for the fine mesh $l_\mathrm{e}/L = 1/8$. No damage localization in single element layers for fine meshes is detected, which indicates the non-local character of the regularized damage model.

4 CONCLUSIONS

A rather simple model to express the asymmetric behavior (strain hardening, martensite evolution) during monotonic, uni-axial tension and compression loading of TRIP-steel is proposed. Experimental data can be fitted well.

A local damage model based on the effective stress concept is applied. Damage evolution is modeled by a modified Rice and Tracey [10] description of void growth. Void coalescence and the linked accelerated damage evolution up to crack initiation are tackled by a phenomenological approach. Cell model predictions of damaged TRIP-steel can be successfully fitted in terms of macroscopic stress-strain curves.

A non-local extension based on a regularization technique is incorporated. A convergence study proves the non-local properties of the proposal.

ACKNOWLEDGMENTS

The authors gratefully acknowledge the German Research Foundation (DFG) for supporting this work carried out in the framework of the Collaborative Research Center 799 (subproject C5). We gratefully acknowledge Ralf Eckner and Michael Hauser (IWT & IEST, TU Bergakademie Freiberg) for providing the experimental data.

APPENDIX

The definition of e_smooth in Eq. (27) should ensure a transition at triaxiality $h = h_\mathrm{t}$ which is smooth differentiable with respect to h. A saturation of the exponential term in Eq. (27) is desired, which starts at $h = h_\mathrm{t}$ and reaches its final value e_max at the prescribed triaxiality parameter h_max:

$$
\begin{aligned}
e_\mathrm{smooth} &= e_\mathrm{max}\left(1 - \exp\left(\frac{e_\mathrm{c}}{h_1\,(e_\mathrm{max} - e_\mathrm{c})}\,(h_\mathrm{t} - h) + \ln\left(\frac{(e_\mathrm{max} - e_\mathrm{c})}{e_\mathrm{max}}\right)\right)\right), \\
e_\mathrm{max} &= \exp\left(h_\mathrm{max}/h_1\right), \\
e_\mathrm{c} &= \exp\left(h_\mathrm{t}/h_1\right).
\end{aligned}
$$

REFERENCES

[1] A. M. Beese and D. Mohr. Anisotropic plasticity model coupled with Lode angle dependent strain-induced transformation kinetics law . *Journal of the Mechanics and Physics of Solids*, 60:1922–1940, 2012.

[2] M. P. Miller and D. L. McDowell. Modeling large strain multiaxial effects in fcc polycrystals. *International Journal of Plasticity*, 12(9):875–902, 1996.

[3] C. Garion, B. Skoczen, and S. Sgobba. Constitutive modelling and identification of parameters of the plastic strain-induced martensitic transformation in 316L stainless steel at cryogenic temperatures . *International Journal of Plasticity*, 22:1234–1264, 2006.

[4] A. Seupel and M. Kuna. Application of a Local Continuum Damage Model to Porous TRIP-Steel. *Applied Mechanics and Materials*, 784:484–491, 2015.

[5] G. B. Olson and M. Cohen. Kinetics of strain-induced martensitic nucleation. *Metallurgical Transactions A*, 6A:791–795, 1975.

[6] T. Iwamoto, T. Tsuta, and Y. Tomita. Investigation on deformation mode dependence of strain-induced martensitic transformation in TRIP steels and modelling of transformation kinetics. *International Journal of Mechanical Sciences*, 40:173–182, 1998.

[7] S. Martin, S. Wolf, S. Decker, L. Krüger, and U. Martin. Deformation Bands in High-Alloy Austenitic 16Cr6Mn6Ni TRIP Steel: Phase Transformation and Its Consequences on Strain Hardening at Room Temperature. *Steel Research International*, 86(10):1187–1196, 2015.

[8] D. Kulawinski, S. Ackermann, A. Seupel, T. Lippmann, S. Henkel, M. Kuna, A. Weidner, and H. Biermann. Deformation and strain hardening behavior of powder metallurgical TRIP steel under quasi-static biaxial-planar loading . *Materials Science & Engineering A*, 642:317–329, 2015.

[9] J. C. Simo and T. J. R. Hughes. *Computational Inelasticity*. Springer, 1998.

[10] J. R. Rice and D. M. Tracey. On the ductile enlargement of voids in triaxial stress fields. *Journal of the Mechanics and Physics of Solids*, 17:201–217, 1969.

[11] T. Linse., G. Hütter, and M. Kuna. Simulation of crack propagation using a gradient-enriched ductile damage model based on dilatational strain. *Engineering Fracture Mechanics*, 95:13–28, 2012.

[12] A. Seupel, R. Eckner, A. Burgold, M. Kuna, and L. Krüger. Experimental characterization and damage modeling of a particle reinforced TWIP-steel matrix composite. *Materials Science & Engineering A*, 662:342–355, 2016.

[13] M. Hauser, M. Wendler, S. Ghosh Chowdhury, A. Weiß, and J. Mola. Quantification of deformation induced a'- martensite in Fe-19Cr-3Mn-4Ni-0.15C- 0.15N austenitic steel by in situ magnetic measurements . *Materials Science and Technology*, 31(12):1473–1478, 2015.

[14] M. Kuna and D. Z. Sun. Three-dimensional cell model analyses of void growth in ductile metals. *International Journal of Fracture*, 81:235–258, 1996.